Author(s): Ihalainen, Janne; Gustavsson, Emil; Schröder, Lea; Donnini, Serena; Lehtivuori, Heli; Isaksson, Linnéa; Thöing, Christian; Modi, Vaibhav; Berntsson, Oskar; Stucki-Buchli, Brigitte; Liukkonen, Alli; Häkkänen, Heikki; Kalenius, Elina; Westenhoff, Sebastian; Kottke, Tilman

Title: Chromophore-Protein Interplay During the Phytochrome Photocycle Revealed by Step-Scan FTIR Spectroscopy

Year: 2018

Version: Accepted version (Final draft)

Please cite the original version:

Ihalainen, J., Gustavsson, E., Schröder, L., Donnini, S., Lehtivuori, H., Isaksson, L., Thöing, C., Modi, V., Berntsson, O., Stucki-Buchli, B., Liukkonen, A., Häkkänen, H., Kalenius, E., Westenhoff, S., & Kottke, T. (2018). Chromophore-Protein Interplay During the Phytochrome Photocycle Revealed by Step-Scan FTIR Spectroscopy. Journal of the American Chemical Society, 140(39), 12396-12404. https://doi.org/10.1021/jacs.8b04659

Article

Chromophore-Protein Interplay During the Phytochrome Photocycle Revealed by Step-Scan FTIR Spectroscopy

Janne A. Ihalainen, Emil Gustavsson, Lea Schröder, Serena Donnini, Heli Lehtivuori, Linnéa Isaksson, Christian Thöing, Vaibhav Modi, Oskar Berntsson, Brigitte Stucki-Buchli, Alli Liukkonen, Heikki Häkkänen, Elina Kalenius, Sebastian Westenhoff, and Tilman Kottke

J. Am. Chem. Soc., **Just Accepted Manuscript** • DOI: 10.1021/jacs.8b04659 • Publication Date (Web): 05 Sep 2018

Chromophore-Protein Interplay During the Phytochrome Photocycle Revealed by Step-Scan FTIR Spectroscopy

Janne A. Ihalainen[1,*], Emil Gustavsson[2,†], Lea Schroeder[3,†], Serena Donnini[1], Heli Lehtivuori[4], Linnéa Isaksson[2], Christian Thöing[3], Vaibhav Modi[5], Oskar Berntsson[2], Brigitte Stucki-Buchli[1], Alli Liukkonen[1], Heikki Häkkänen[1], Elina Kalenius[5], Sebastian Westenhoff[2,*], Tilman Kottke[3,*]

1) University of Jyväskylä, Nanoscience Center, Department of Biological and Environmental Science, Jyväskylä, 40014 Finland
2) University of Gothenburg, Department of Chemistry and Molecular Biology, Gothenburg, 40530 Sweden
3) Bielefeld University, Physical and Biophysical Chemistry, Universitätsstr. 25, 33615 Bielefeld, Germany
4) University of Jyväskylä, Nanoscience Center, Department of Physics, Jyväskylä, 40014 Finland
5) University of Jyväskylä, Nanoscience Center, Department of Chemistry, Jyväskylä, 40014 Finland

*Corresponding authors; email: janne.ihalainen@jyu.fi, westenho@chem.gu.se, tilman.kottke@uni-bielefeld.de

†These authors contributed equally to this work

Abstract

Phytochrome proteins regulate many photoresponses of plants and microorganisms. Light absorption causes isomerization of the biliverdin chromophore, which triggers a series of structural changes to activate the signaling domains of the protein. However, the structural changes are elusive and therefore the molecular mechanism of signal transduction remains poorly understood. Here, we apply two-color step-scan infrared spectroscopy to the bacteriophytochrome from *Deinococcus radiodurans*. We show by recordings in H_2O and D_2O that the hydrogen bonds to the biliverdin D-ring carbonyl become disordered in the first intermediate (Lumi-R) forming a dynamic microenvironment, then completely detach in the second intermediate (Meta-R), and finally reform in the signaling state (Pfr). The spectra reveal via isotope labeling that the refolding of the conserved 'PHY-tongue' region occurs with the last transition between Meta-R and Pfr. Additional changes in the protein backbone are detected already within microseconds in Lumi-R. Aided by molecular dynamics simulations, we find that a strictly conserved salt bridge between an arginine of the PHY tongue and an aspartate of the chromophore binding domains is broken in Lumi-R and the arginine is recruited to the D-ring C=O. This rationalizes how isomerization of the chromophore is linked to the global structural rearrangement in the sensory receptor. Our findings advance the structural understanding of phytochrome photoactivation.

Introduction

Phytochromes are photosensory proteins in plants, fungi, algae and bacteria,[1–5] regulating vital light and temperature responses.[6–8] They function by converting light cues into a structural signal, perturbing the protein structure and modulating its biochemical activity. Phytochromes widely share a conserved photosensory core, consisting of the three domains Per/ARNT/Sim (PAS), cyclic guanosine monophosphate phosphodiesterase/adenylyl cyclase/FhlA (GAF), and phytochrome-specific (PHY) (Figure 1a). In bacterial phytochromes, the output domains are connected to the C-terminus of the PHY domain and a biliverdin chromophore is bound to the PAS domain (Figure 1b).[9]

Phytochromes can be photoconverted between two states, which are termed Pr and Pfr. Most phytochromes thermally relax to Pr in the dark within minutes to days. The photoconversion from the Pr to Pfr involves at least two intermediate states, called Lumi-R and Meta-R, and takes 1 to 1000 milliseconds, depending on the species (Figure 1c).[10–15] The photoinduced Pfr→Pr -reaction proceeds via Lumi-F and Meta-F states. Inferred from observations on a cyanobacterial and a bacterial phytochrome, the Meta-R state involves proton exchange between the chromophore, protein, and solvent,[13,14] but the bilin molecule is fully protonated in Pr and Pfr.[16]

Atomic structures of the photosensory core in Pr and Pfr states have been revealed by X-ray crystallography and NMR spectroscopy.[17–25] The structural differences between Pr and Pfr include different chromophore conformations and associated changes of several residues in the PAS-GAF domains, for example H290 and Y263 (numbering refers to the phytochrome from *D. radiodurans*) (Figure 1b).[20,23,26,27] In Pr, a conserved salt bridge between R466 and D207 forms the most direct connection between the chromophore and the so-called "tongue" of the PHY domain, but in Pfr the salt bridge is absent. The tongue has different folds between Pr and Pfr.[18,19,21,23] Global structural changes of the entire phytochrome have been reported,[28,29] probably mediated by the coiled-coil spline helices.[25]

Even though the structures of the Pr and Pfr states are available and the photocycle is determined, the structural changes associated with the intermediate states remain poorly understood. It is clear that the Pr→Pfr and Pfr→Pr reactions follow different molecular mechanisms.[30] In both cases isomerization around the C15=C16 bond of the chromophore is the first step of photoconversion. The structures of the chromophore and some nearby amino acids have been revealed by crystallographic analysis of cryo-trapped intermediates along the Pfr→Pr reaction.[31] Similar, a structural model of the chromophore binding pocket has been obtained for cryo-trapped Lumi-F and Meta-F intermediates by NMR spectroscopy.[32]

The structural details of the intermediates along the Pr→Pfr transition are largely unresolved. Time-resolved X-ray solution scattering[21,28] and transient grating measurements[33] have revealed global changes of the full-length phytochromes, but they lack spatial resolution for atomic details. Vibrational spectra of cryo-trapped Lumi-R and Meta-R intermediates have been analyzed.[30,34–37] Ultrafast infrared spectroscopy at room

temperature has been used to track the isomerization reaction of the chromophore and to record a spectrum of the Lumi-R state in D_2O.[26,38] Moreover, the vibrational spectrum of the Meta-R_c state has been reported by means of rapid-scan FTIR spectroscopy.[36] Nevertheless, the structural insight has been limited by difficulties to connect spectroscopic signals to structural changes.

For both the Pfr→Pr and Pr→Pfr reactions it is currently unclear how the isomerization of the chromophore leads to signal transfer in the protein. A focal point ought to be to find out how the salt bridge R466:D207 is broken, which is a hallmark of all Pr crystal structures,[18,21,22,24] because this would free the tongue for refolding. It has been suggested that this occurs by a transient protonation of the D207 side chain,[16] but this hypothesis remains untested.

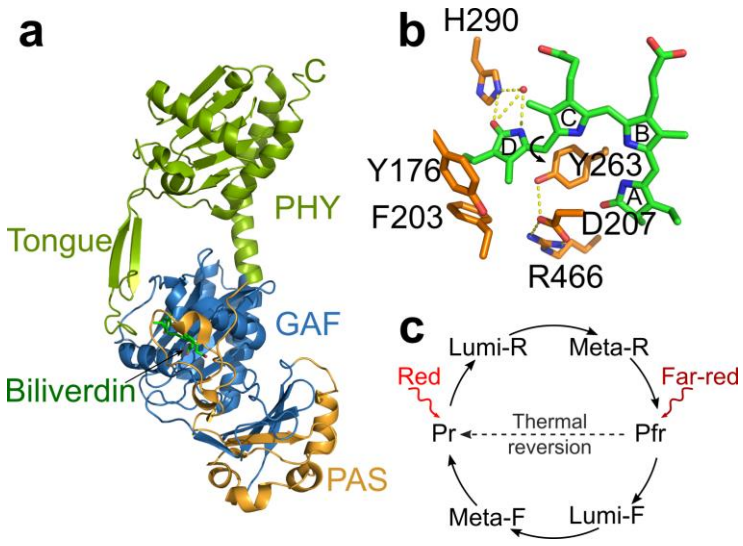

Figure 1. The photosensory core of phytochromes. (a) The sensory module comprises the PAS-GAF-PHY domains, as depicted for a monomer of the bacteriophytochrome from *D. radiodurans* (pdb accession code: 4O0P)[21]. The output domain (not depicted) is located C-terminally of the PHY domain, marked C. (b) The module binds a biliverdin as a chromophore. Key amino acids are included in the representation of the Pr state (pdb accession code: 4Q0J).[29] The water molecule involved in the interaction of the D-ring is indicated as a red sphere. (c) Upon red light absorption, the phytochrome from *D. radiodurans* undergoes a photocycle that can be reverted by far-red light.

To gain insight into the molecular changes on nano- to millisecond timescales, we use step-scan FTIR spectroscopy.[39,40] The data are recorded at room temperature. This is an advantage over cryo-trapping as biologically relevant dynamics within the intermediate states are accessible.[41] The step-scan technique has been successfully applied to several other sensory photoreceptors,[42–46] light-driven ion pumps,[47,48] photosynthetic reaction centers,[49] and a complex of the respiratory chain,[50] but, to the best of our knowledge, not to phytochromes.[36] Typically, phytochromes complete the photoreaction within about 800 ms and the thermal back reversion can take up to days.[7,21] These rates prevent full recovery of the resting state within a reasonable time for spectra processing in step-scan spectroscopy.

Here, we overcome this hurdle by using the *Deinococcus radiodurans* phytochrome with its faster (Pr→Pfr) reaction and by driving the protein back to the Pr state using a far-red laser flash,[21,28,51] thereby establishing a novel approach of two-color step-scan FTIR spectroscopy. While such an approach has been applied previously to other time-resolved techniques, photochromism has, to our knowledge, not been exploited in step-scan FTIR spectroscopy. The challenge is the inherent sensitivity to smallest variations in sample recovery when initiating the reaction at different interferometer positions. The approach allowed us to measure spectra in the micro- to millisecond time range with low noise levels and to reveal how the carbonyl groups of the bilin molecule, specific elements of secondary structure, and side chains undergo decisive changes during the multistep photoreaction.

Results and Discussion

The Photocycle as Revealed by Step-Scan FTIR Spectroscopy. We recorded time-resolved step-scan FTIR spectra of the monomeric[52] and dimeric PAS-GAF-PHY photosensory module of the phytochrome from *Deinococcus radiodurans* (*Dr*BphP$_{PSM}$). A 10-ns laser pulse at 660 nm initiated the photoreaction. After completion of the spectral evolution, the protein was driven back to the Pr state using a laser flash at 751 nm (40 ms duration) and full recovery was confirmed (Figure S1). The transient infrared spectra were fitted globally to a model of sequential reactions to obtain three species-associated difference spectra (SADS) (Figure 2a) with lifetimes of 77 μs, 1.46 ms and >5 ms (Figure 2b). The SADS are confirmed by extracting spectra from the raw data in characteristic time windows (Figure S2). The final SADS (> 5 ms) agrees very well with the Pfr *minus* Pr steady-state spectrum (Figure 2a), which confirms that the Pfr state is reached within the allotted time. In particular, the Meta-R$_a$ and Meta-R$_c$ substates, detected for the phytochromes from *Agrobacterium fabrum* and *Synechocystis sp. PCC 6803*,[13,14] were not separated in our time-resolved infrared spectra.

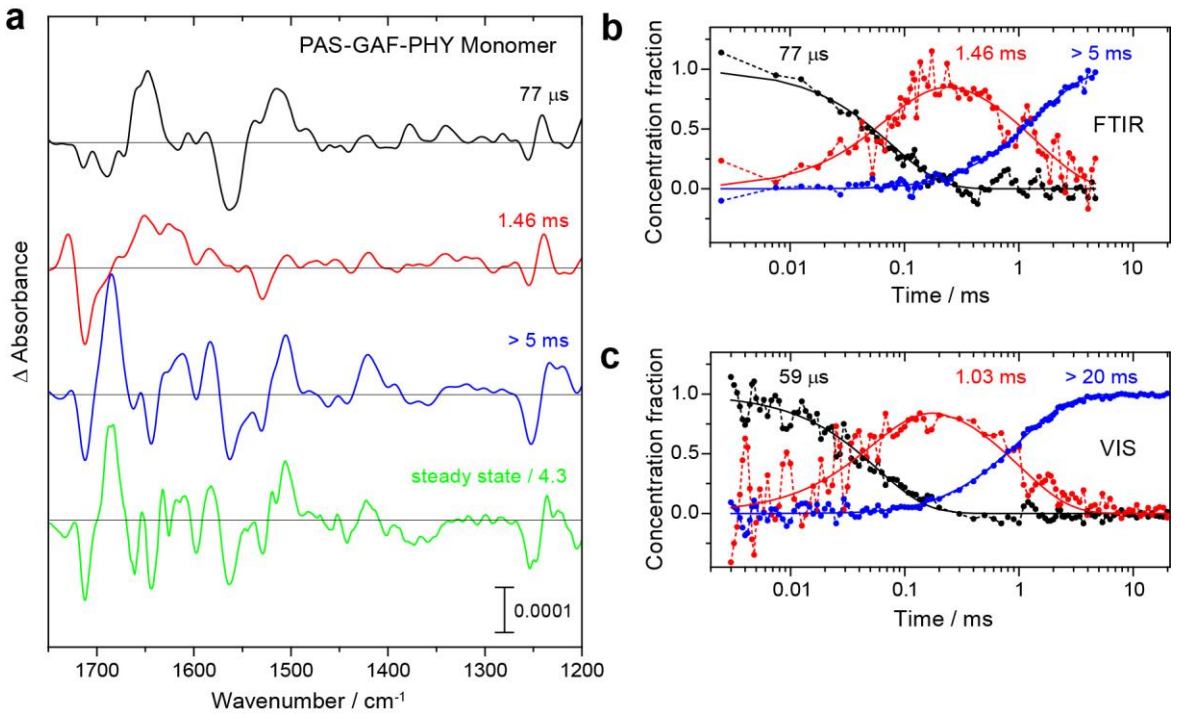

Figure 2. Time-resolved infrared spectra of the *Dr*BphP$_{PSM}$ photoreaction. (a) The global analysis of step-scan FTIR spectroscopic data of *Dr*BphP$_{PSM}$ yields species-associated difference spectra (SADS) for three components. SADS for monomeric PAS-GAF-PHY domains are shown. The steady-state FTIR difference spectra of Pfr *minus* Pr are included at the bottom (green). The positive signals represent the induced absorption in the intermediate and product states whereas the negative signals correspond to the disappearance of absorption from the initial, Pr state. Note that the spectral resolution of the steady-state spectra is higher (2 cm^{-1}) than those from step-scan (8 cm^{-1}). (b) The concentration fraction of each species was derived as a function of time from the global fit of the FTIR data. Comparing the data (dots) to the fit (line) indicates excellent agreement. (c) Global analysis of flash photolysis data of dimeric PAS-GAF-PHY yields the concentration fraction evolution of the three species in the visible for comparison. A more throughout analysis of the flash photolysis data is presented in[28].

Comparison to previously determined lifetimes in the visible spectral range by flash photolysis of 59 µs, 1.03 ms and >20 ms reveals excellent agreement (Figure 2c).[21,28] From this comparison we infer that the three SADS from FTIR (Figures 2a and 2b) represent the Lumi-R, Meta-R and Pfr states.[28] The monomeric and dimeric protein variants show very similar spectral features and kinetics (Figure S3). We will concentrate on the monomeric *Dr*BphP$_{PSM}$ in this paper, because it provided the most clear and homogenous data.

Assignment of Signals in the Carbonyl Spectral Region Reveals that D207 is not Transiently Protonated in the Pr→Pfr Reaction. We used uniformly $^{13}C^{15}N$-labeled protein with non-labeled biliverdin (Figure S4) to separate the chromophore and protein peaks. The labeling downshifts the amide I and II modes of the protein backbone by about 45 cm^{-1} and 19 cm^{-1}, respectively (Figure S6a), concomitant with shifts of the side chain modes that include C and/or N atoms. The vibrational frequencies of biliverdin remain

largely unaffected. In the region of carbonyl stretches (Figures 3a and 3b), most peaks are insensitive to isotope labeling and therefore originate from biliverdin. Following previous assignments,[34] the negative peaks at 1737 cm^{-1} and 1714/1712 cm^{-1} originate from the carbonyl vibrations of the A-ring (C_1=O) and D-ring (C_{19}=O) in Pr, respectively. Shifts due to H/D exchange are indicative of the H-bonding strength of the carbonyl group. The two peaks downshift in D_2O by, respectively, 7 cm^{-1} and 12 cm^{-1} (Figure 3d), which indicates a somewhat tighter hydrogen bonding coordination of the D-ring C=O compared to that of the A-ring.

The final (Pfr) spectrum (Figure 3d) reveals positive chromophore peaks at 1726 cm^{-1} and 1685 cm^{-1}. The strongly different band intensities support their assignment to the A- and D-ring carbonyls, respectively. The D-ring carbonyl stretch in Pfr is downshifted by >10 cm^{-1} compared to a "bathy" bacteriophytochrome, which has Pfr as the resting state.[53,54] A small negative indentation in the Pfr spectrum at ~1695 cm^{-1} originates from the protein, because it shifts with $^{13}C^{15}N$ labeling out of the displayed spectral window (Figure S5). A downshift by H/D exchange of ~8 cm^{-1} indicates moderate hydrogen bonding to the C=O groups in Pfr (Figure 3d).

The Meta-R spectrum has a positive band at 1730 cm^{-1} (Figure 3e). Figure 3c explicitly demonstrates that the peak rises and decays with the Meta-R state. The absence of a shift by labeling of the protein with $^{13}C^{15}N$ confirms that the peak originates from the chromophore. The propionic acids of the chromophore are excluded as candidates by the low frequency of the band[53] and by the small shift by 5 cm^{-1} upon H/D exchange (Figure 3e). We exclude a protonated aspartic acid as an origin for the peak as we did not detect any shift >1700 cm^{-1} in a sample with all aspartic acids labeled with $^{13}C_4$ compared to the unlabeled sample (Figure 3e). Thus, we assign the 1730 cm^{-1} band to the D-ring (C_{19}=O). This is in agreement with assignments on plant phytochrome A.[34] The observed small H/D shift is fully accounted for by H/D exchange at the biliverdin pyrrole N-H, which we calculate to result in a downshift of the carbonyl band by 5 cm^{-1} (Figure S6b). This means that the carbonyl of the D-ring has very weak, if any, hydrogen bond in Meta-R. A rate-limiting (de)protonation event in the formation and decay of Meta-R is unlikely considering the minor changes in kinetics of the D-ring carbonyl signal in H_2O with $\tau_{formation}$ = 77 μs and τ_{decay} = 1.46 ms (Figure 3c) as compared to D_2O with $\tau_{formation}$ = 130 μs and τ_{decay} = 1.67 ms (Figure 3f).[55]

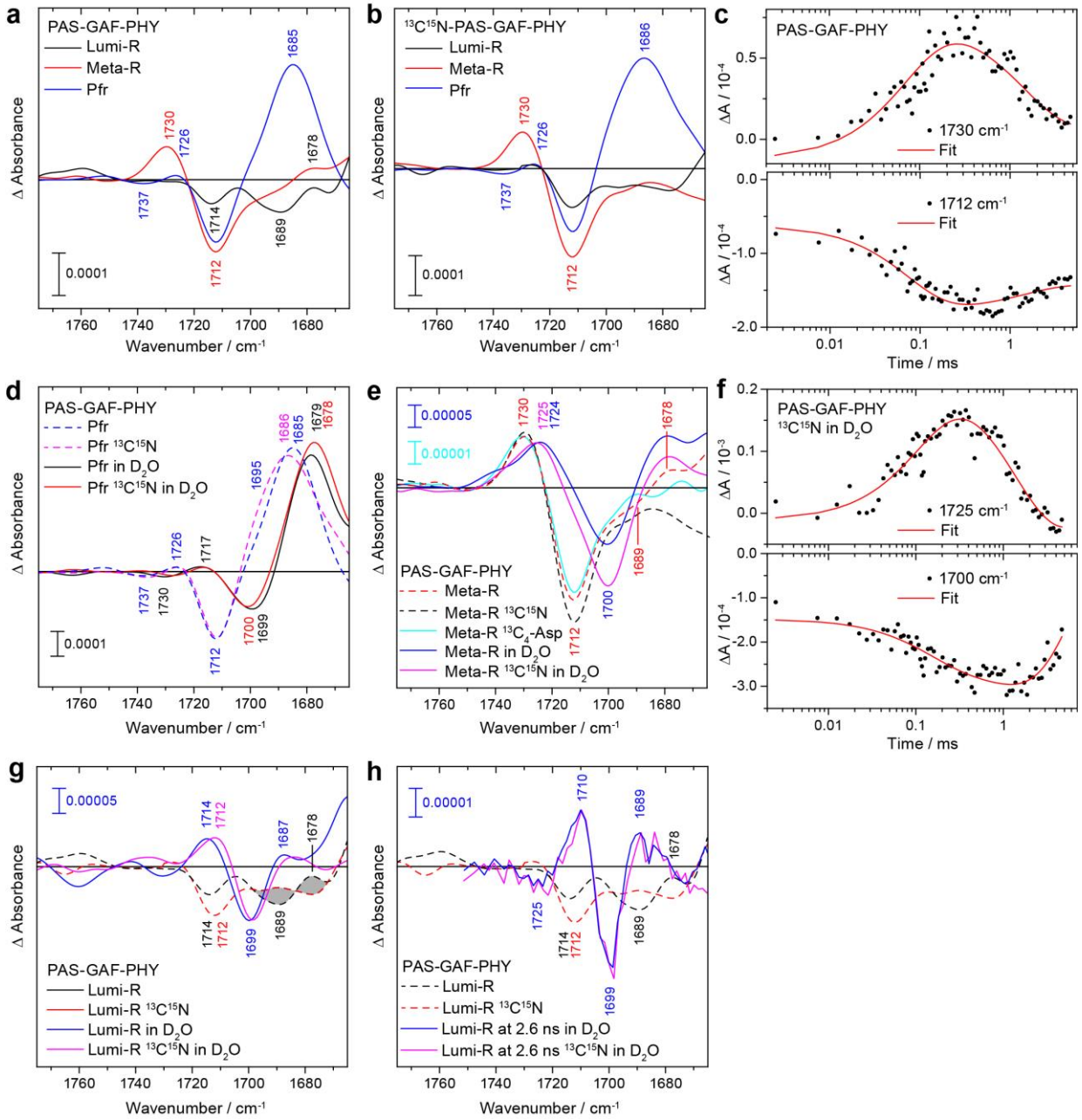

Figure 3. Biliverdin-specific changes in carbonyl vibrations compared to Pr in the monomeric *Dr*BphP$_{PSM}$. (a) The spectral range of carbonyl vibrations of non-labeled samples is zoomed from Figure 2. (b) Signals from the protein moiety are shifted by selective $^{13}C^{15}N$-labeling, whereas the biliverdin remained at natural abundance. (c) The kinetic traces of the raw data at 1730 cm^{-1} and 1712 cm^{-1} visualize strong changes at the biliverdin carbonyls over the photocycle. The lower panels show the transient difference spectra in D_2O for Pfr (d), Meta-R (e) and Lumi-R (g) states. Both $^{13}C^{15}N$-labeled and non-labeled samples were investigated and scaled at 1700 cm^{-1} and 1725 cm^{-1}, respectively. For comparison, spectra in H_2O from upper panels were included as dashed lines. (e) Bands in the Meta-R spectrum have been assigned with the help of a $^{13}C_4$-Asp-labeled dimeric sample. (f) The kinetic traces of the raw data at 1725 cm^{-1} and 1700 cm^{-1} of a $^{13}C^{15}N$-labeled sample in D_2O visualize the absence of a pronounced kinetic isotope effect. (g) The Lumi-R spectrum shows a difference band highlighted in grey which is lost in D_2O and upon $^{13}C^{15}N$-labeling. Deviations from the baseline at above 1740 cm^{-1} are attributed to an increase in noise caused by the band-pass filter. (h) Pump-probe experiments at 2.6 ns in D_2O with higher spectral resolution are included and scaled at 1710 cm^{-1}. In all spectra,

negative signals originate from the conversion of Pr, the assignment of the positive signals to the respective intermediates are indicated.

Importantly, our assignments explicitly exclude that transient protonation of the D207 side chain occurs in any of the intermediates of the Pr→Pfr photoreaction. If this were the case, a prominent peak would have been expected in the spectral range from 1710 cm^{-1} to 1760 cm^{-1} (Figures 3a and 3b). Our specific labeling of all aspartic acids demonstrates that the only candidate peak, which we observe at 1730cm^{-1} in the Meta-R spectrum, is not due to an aspartic acid.

The D-Ring Carbonyl has a Dynamic Environment in Lumi-R. The step-scan spectra of the Lumi-R state (Figure 3g) are intriguing because the positive peak of the D-ring carbonyl is missing and the negative band at 1714 cm^{-1} (1712 cm^{-1} in the $^{13}C^{15}N$-labeled sample) has a strongly reduced intensity as compared to Meta-R or Pfr (Figure 3a). This spectral evolution can only be explained by a situation in that a broad photoinduced absorption in Lumi-R overlaps with the bleach, partially cancelling each other out. Indeed, in the Lumi-R spectrum in D_2O, positive wings become visible around the downshifted negative peak of the D-ring carbonyl at 1699 cm^{-1}. Thus, we conclude that the band of the C=O vibration of the D-ring in Lumi-R is broadened. This indicates that the D-ring carbonyl experiences a dynamic chemical environment in Lumi-R.

To back this assignment up, we recorded a spectrum of Lumi-R at an earlier time point of 2.6 ns using a femtosecond pump-probe setup (Figure 3h). The data were recorded in D_2O and thus the negative band locates at 1699 cm^{-1}. We achieved a higher spectral resolution of 2 cm^{-1} with pump-probe spectroscopy as compared to 8 cm^{-1} in the step-scan spectra. The spectra agree very well in the range >1690 cm^{-1} after accounting for the difference in resolution (Figure S7). Figure S7 also indicates some spectral differences between Lumi-R at 2.6 ns (pump-probe) and in the microsecond range (step-scan) at < 1690 cm^{-1}. This may indicate that the Lumi-R state evolves on the nanosecond time scale. At the higher resolution of pump-probe spectroscopy, the positive sidebands flanking the D-ring C=O peak become even more visible at 1710 cm^{-1} and 1689 cm^{-1} confirming the existence of a photoinduced, broadened carbonyl peak in Lumi-R (Figure 3h). The two positive peaks are attributed to either a single broad positive band, which overlaps with the bleach because of a similar frequency, or to two positive peaks, which appear on both flanks of the spectral position of the bleach.

Although our assignments for the Pr, Pfr, and Meta-R states are in good agreement with assignments for cryo-trapped spectra of a plant phytochrome from *Avena sativa,*[30,34] the Lumi-R state is an exception. In the cryo-trapped Lumi-R spectrum, a sharp positive peak was observed and assigned to the D-ring C=O group. Our spectra at room temperature reveal a broad feature (Figures 3g and h). This observation is in agreement with a Lumi-R spectrum recorded at around 1 ns of a cyanobacterial phytochrome, which shows a similar broad pattern but with about 20 cm^{-1} upshifted C=O vibrational frequencies.[38] This comparison indicates that dynamics present at biologically relevant temperatures are 'frozen out' in the cryo-experiment.

In addition, the step-scan Lumi-R spectrum reveals a peak pair at 1689(-) / 1678(+) cm^{-1} (Figure 3g, highlighted in grey). The pair originates from the protein, because it shifts out of the presented spectral window upon labeling with $^{13}C^{15}N$. Moreover, the peaks are also shifted out of this spectral window by H/D exchange (Figures 3g and 3h), which excludes backbone contributions (amide I) as an origin. The most likely candidate for this spectral signature is the C-N vibrations of an Arg guanidinium group. This signal would downshift by ~30 cm^{-1} upon $^{13}C^{15}N$-labeling (Figure S6c) and by 60-80 cm^{-1} in D_2O.[56] The shifted peaks stay, however, unidentified from the labeled step-scan data or from pump-probe spectra, because they overlap with contributions from H_2O and amide I' signals, respectively. A similar peak pair (1689(-) / 1678(+) cm^{-1}) is detected in the Meta-R spectrum (Figure 3e), whereas the Pfr spectrum reveals only a negative contribution at ~1686 cm^{-1} (Figure S5b). It should be noted that a Gln or Asn side chain cannot be fully excluded as candidates for this signal.[57]

Structural Model of the Lumi-R State. To place the spectroscopic findings in a structural perspective, we generated molecular dynamics (MD) trajectories starting from the crystal structures of the Pr (trajectory length 500 ns) and Pfr (500 ns) states,[22,23] and from simulated structures of the Lumi-R state (multiple simulations totaling 3500 ns). The Lumi-R structures were obtained by rotating the biliverdin D-ring of the Pr structure clockwise around the dihedral C4C-CHD-C1D-ND (Figure S8) during 100 ps of force probe simulations.[58] The resulting dihedral angles between -159 degrees and -167 degrees are in agreement with the -172 degrees, which were determined using polarization-resolved infrared spectroscopy for the chromophore in Lumi-R state in the phytochrome from *Synechocystis sp. PCC* 6803.[26] The dihedral angle is also consistent with the Pfr crystal structures of the *D. radiodurans* phytochrome (Figure S8). We found that this conformation is reached by most simulations only when using clockwise rotation, not anti-clockwise rotation, in agreement with CD measurements of Rockwell *et al.*[59] All other residues relaxed freely in response to the new chromophore conformation.

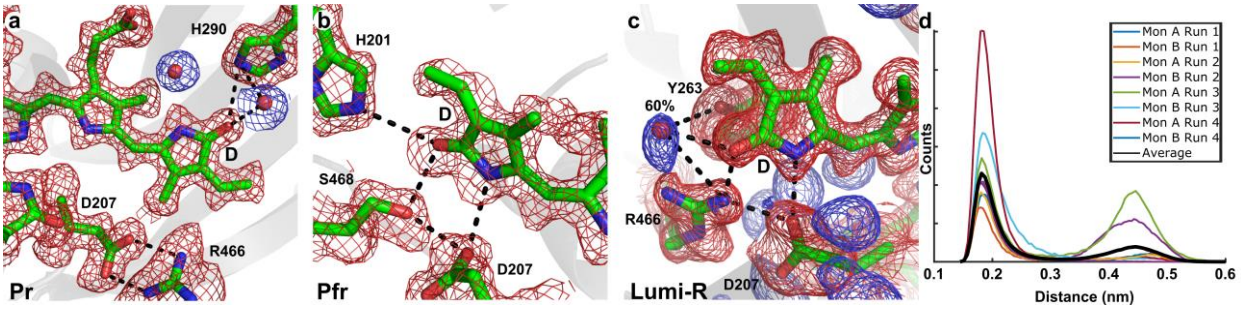

Figure 4. The structure of the chromophore binding pocket as revealed by molecular dynamics simulations of *Dr*BphP$_{PSM}$. The electron density (mesh) averaged over the trajectory (see main text) is shown together with a structure fitted to the density with real-space refinement for Pr (a), Pfr (b), and Lumi-R (c) states. The red mesh represents electron density of the biliverdin and amino acids and the blue mesh indicates water molecules. (d) The distance distribution between the D-ring C=O and the closest water molecule for the Lumi-R trajectory is bimodal indicating a dynamic structure.

Figure 4a-4c shows electron densities, which were obtained by averaging the electron densities of all frames after aligning on the biliverdin rings A-C. In this representation, the intensity of the resulting densities reflect the occupancy and disorder of the atoms. The average simulated structure for Pr shows that the D-ring C=O forms H-bonds with H290 (3.2 Å) and a water molecule (Figure 4a),[60] in agreement with the crystal structure.[21,22] The hydrogen bond pattern is also in qualitative agreement with the infrared spectra (Figure 3d), which indicate considerable hydrogen bonding strength in Pr. The strong electron density of the water molecules (blue in Figure 4) indicates that they are stationary in the Pr trajectory. In agreement with the crystal structures,[21,22] D207 forms a stable salt bridge to R466.

In Pfr, the D-ring C=O has a stable H-bond to H201 (3.2 Å, Figure 4b), as also observed in the crystal structure.[23] Moreover, a H-bond between S468 of the PHY tongue and D-ring C=O is also observed. This bonding pattern is in agreement with the infrared spectra (Figure 3d), where we concluded on moderate hydrogen bonding. D207 forms a stable H-bond to the N-H of the D-ring. Overall, the Pr and Pfr states agree with the crystal structures and are rather stable in the simulations. This is in line with the narrow peaks detected in the infrared spectra of the states (Figure 3).

Differing from the Pr and Pfr conformations, the Lumi-R trajectories indicate highly dynamic H-bonding patterns for the D-ring C=O. The functional group is bound to one or two of the NH-groups of R466 (Figures 4c and S11) and to a water molecule, which is present in 60 % of the simulated frames (Figure 4d). The water is also in hydrogen bonding distance to the conserved Y263. The hydrogen bond between the D-ring C=O and R466 was observed in all four long simulations (of length 1000 ns, 1000 ns, 500 ns, and 500 ns, Figure S13) and the dynamic water was also present in all trajectories, albeit the occupancies varied (Figure 4d). The water is recurring several times in the course of a simulation, much faster than the lifetime of the Lumi-R state (Figure S9, Movie S1). From the MD trajectories, we also estimated the electric field[61] acting on the D-ring C=O group and found that the distribution is significantly broader in Lumi-R compared to Pr and Pfr (Figure S12). All of these findings are in excellent agreement with the detected broad or distributed shape of the D-ring carbonyl peak in the IR spectra of the Lumi-R state (Figures 3g and h).

Further support for the model is provided by the peak pair at 1689(-) / 1678(+) cm^{-1}, observed in the Lumi-R spectrum (Figure 3g). The peaks indicate a change in the chemical environment of an arginine side chain. Indeed, the model shows that R466 changes from being part of the salt bridge to D207 in Pr (Figure 4a) to forming a cyclic cluster involving D207 and the NH and C=O groups of the biliverdin D-ring in Lumi-R (Figure 4c). The lowering in frequency in the experiment is in agreement with a change from the salt bridge to weaker interactions.[56] Since the peak pair is also seen in the Meta-R spectrum (Figure 3e), we conclude that the change around the arginine residue persists in Meta-R. In Pfr, we only observed the negative part of the peak pair (Figure S5b), which is in agreement with the crystal structures in Pfr, where R466 points towards the solvent resulting in a broadened and shifted signal. Moreover, we tentatively assign signals at 1468(-) / 1484(+) cm^{-1} to the

corresponding upshift of the asymmetric COO^- stretch of D207 (Figure 5a and S6c). The peak pair is downshifted by -17 cm^{-1} in the $^{13}C^{15}N$-labeled sample (Figure 5a).

The Lumi-R simulation also reveals that biliverdin isomerization causes rotation of Y176 together with movement of F203, freeing space for H201 to move towards the chromophore (Figures S11 and S15). This is consistent with the expected position of the residues in Pfr (Figure S11c),[23] providing support to the reliability of the structural model and showing that the Y176 position directly correlates with the position of the D-ring. We observed that Y176 is connected to the D207-R466/D-ring network via a stable water molecule (Figure S11b).

Taken together, our FTIR data exclude that D207 is transiently protonated. Instead, the MD model based on the FTIR data indicates that R466 and D207 are recruited to the D-ring following isomerization. This leads to breakage up of the D207:R466 salt bridge which transduces the signal to the tongue region.

Conformational Changes of the Protein Backbone Detected Already in Lumi-R. In the following section, we will analyze the amide I and II regions of the spectra as reporters of secondary structure (Figure 5). In structural studies of *Dr*BphP$_{PSM}$, a refolding of a β-sheet into an α-helix was observed in the tongue region.[21] The amide II spectral region is a particularly sensitive reporter of secondary structure as it is uninfluenced by H_2O absorption changes.[62] It reveals prominent contributions at around 1564(-) cm^{-1} and 1508(+) cm^{-1} in the spectra of Lumi-R and Pfr but much weaker signals in Meta-R (Figures 2a and 5a). $^{13}C^{15}N$ labeling downshifts the signals in Lumi-R by 18 cm^{-1} and 23 cm^{-1}, respectively (Figure 5a), in accordance with theory for amide II (Figure S6a). The kinetics of the raw data confirms that conformational changes of protein backbone are detected very early in Lumi-R and later in Pfr, but not in Meta-R (Figure 5b). The observed changes in the amide regions of the Lumi-R state may not represent typical secondary structural changes. Rather, our MD simulations suggest that the backbone changes in the Lumi-R state are small but located overall in the protein regions (Figure S15).

To identify more details about the nature of the structural changes, we inspect the amide I spectral region (1695-1615 cm^{-1}). Signals at 1630(-) / 1653(+) cm^{-1} in Pfr *minus* Pr FTIR spectra have been assigned to the refolding of the tongue region for the phytochrome from *Rhodopseudomonas palustris* (*Rp*Bph).[63] In *Dr*BphP$_{PSM}$ side chain absorptions of the PAS-GAF domain conceal these peaks.[64] Here we show that labeling *Dr*BphP$_{PSM}$ with $^{13}C^{15}N$ downshifts the amide I peaks and they become visible at 1597(-) cm^{-1} and 1612(+) cm^{-1} in the SADS of Pfr (Figure 5c) and the Pfr *minus* Pr steady-state spectrum (Figure S14b). The isotope-induced downshift by 39 cm^{-1} is consistent with the assignment to the β-sheet / α-helix transition.

The amide I spectrum of the early changes in Lumi-R and Meta-R deviate from the changes in Pfr (Figure 5c). In Lumi-R, a small negative peak at 1587 cm^{-1} and a large positive peak at 1616 cm^{-1} are observed. This confirms that backbone structural changes occur already in Lumi-R, however that they are of different nature. The bleach at 1597(-) cm^{-1} in Pfr is indicative of the disappearance of the β-sheet in the tongue. Since this signal is absent in

Lumi-R and Meta-R we conclude that the β-sheet in the tongue, albeit with possible small changes, still exists until the Meta-R state and that the new fold of the tongue develops in the latest step of the photocycle from Meta-R to Pfr.

That the β-sheet of the tongue first disappears in the transition from Meta-R to Pfr is consistent with infrared spectroscopic analyses of Meta-R/Meta-F states, trapped by mutagenesis or at low temperature.[53,63] The associated millisecond time constant is three orders of magnitude longer than the intrinsic formation times of secondary structural elements,[65,66] implying that the inherent unfolding and refolding of the β-sheet and the α-helix, respectively, are not the rate-determining steps. Instead, additional protein structural changes, likely those that affect the interface between GAF and PHY domains,[21,23,24,67] may be rate-limiting. Notable is that structural changes in the histidine kinase output domains occur on the same time scale.[28] Thus the secondary structure of the tongue is a complex function of the structure of the biliverdin binding pocket and the quaternary state of the protein, highlighting the tight coupling between refolding of the PHY-tongue, absorption changes of the biliverdin, and modulation of the output module.

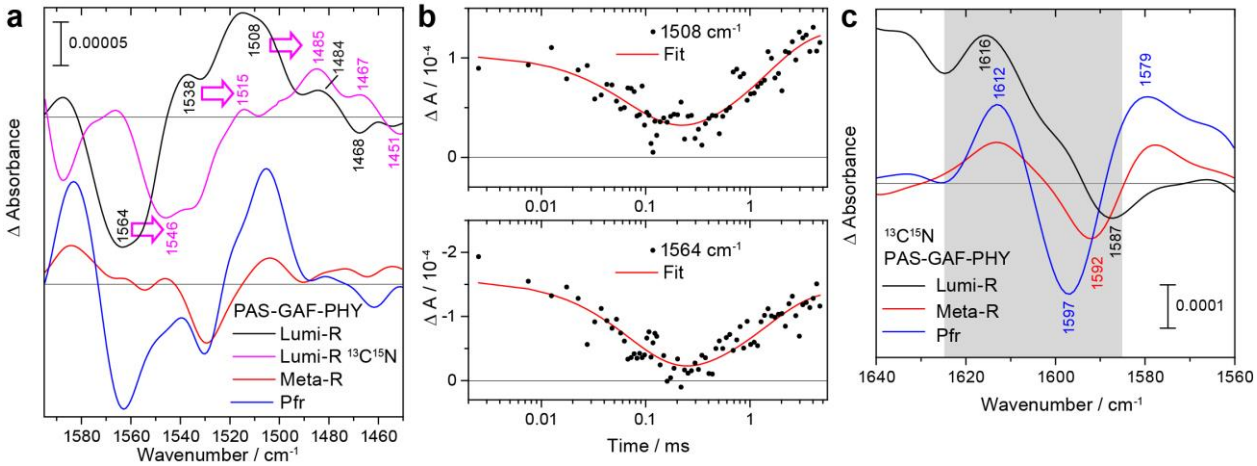

Figure 5. Protein backbone signals in the monomeric *Dr*BphP$_{PSM}$ including the β-sheet to α-helix transition. (a) The amide II signals in Lumi-R, Meta-R, and Pfr states are depicted together with those of the Lumi-R of the $^{13}C^{15}N$-labeled sample (purple) scaled at 1714 cm^{-1}. The characteristic shift upon labeling is indicated by arrows. Additional signals as indicated for the Lumi-R spectra are found below 1500 cm^{-1} at 1468(-) / 1484(+) cm^{-1} and tentatively assigned to an aspartate side chain (b) Kinetics of amide II signals at 1508(+) and 1564(-) cm^{-1} of Lumi-R show a strong decrease of secondary structural changes towards Meta-R followed by an increase. The negative difference absorbance at 1564 cm^{-1} has been inverted for clarity. (c) The amide I region of the SADS of Lumi-R, Meta-R, and Pfr states of the $^{13}C^{15}N$-labeled sample. Signals at 1597 (-) / 1612 (+) in Pfr are indicative of a β-sheet to α-helical transition in the tongue region. Note that the signals are downshifted by 39 cm^{-1} compared to the non-labeled sample (Figure S14b).

Conclusions

The spectra in the carbonyl region (Figure 3) highlight that the biliverdin D-ring carbonyl experiences vastly different chemical environments during the photocycle of the *D.*

radiodurans phytochrome. From Pr to Lumi-R, the H-bonds of the D-ring become disordered. In Meta-R, the H-bonds of the D-ring are very weak or lost. Finally, in Pfr, the H-bond environment is reformed. The spectral signatures of the A-ring carbonyl are much muter. This highlights that the D-ring is the center of action for molecular rearrangements,[21,23,31] but that the A, B, and C rings also adapt to the changes between Pr and Pfr.[23,31]

In absence of structural data for the intermediate states of the Pr→ Pfr photoreaction, our model of the Lumi-R state (Figure 4) provides an explanation on how isomerization of the D-ring couples to the tongue region. We suggest that the D207:R466 salt bridge is replaced by a hydrogen-bonded cluster consisting of the D-ring C=O and NH groups, D207, and R466 (Figure 4c). This event may lead to signal transduction between the chromophore and the C-terminal output domain. Support for the model is provided by the infrared spectra, in particular by the attenuation of the bleach signal of the D-ring carbonyl in Lumi-R (Figure 3a), the broad positive peak associated with the group (Figures 3g and h), and the detected peak pair at 1689(-) / 1678(+) cm^{-1} tentatively assigned to arginine (Figure 3g).[21]

Our data show that refolding of the tongue occurs concomitant to the conversion from Meta-R to Pfr. We also find that prominent changes in the amide I and amide II spectral regions occur much earlier in the photocycle, indicating backbone changes in Lumi-R (Figures 5a and S14d). Although our MD trajectory of Lumi-R revealed some changes in backbone atoms (Figure S15), a definite assignment requires further experiments. It is intriguing that backbone changes occur in Lumi-R and in Pfr, but that the changes are rather muted in Meta-R (Figure 5b).

It is interesting to discuss the structural indicators for the Meta-R state provided by our interpretation of the infrared spectra. The peak pair at 1689(-) / 1678(+) cm^{-1} persist in Meta-R, indicating that the arginine side chain interacts with some binding partner. The binding partner in Meta-R cannot be the D-ring C=O as it is in Lumi-R, because our H/D exchange infrared spectra indicate no hydrogen bonding for the D-ring C=O. We also learned that the tongue remains in its β-sheet form in Meta-R, but it must now be disconnected from the biliverdin. The detected backbone changes in Lumi-R may be preparing the detachment process. It has also been found that the chromophore slides in its binding pocket between Pr and Pfr,[23,31] and it may be that this sliding movement is responsible for the separation of the D-ring C=O from R466 in Meta-R.

We find that the Lumi-R state is highly dynamic in structure, at least at around the D-ring carbonyl. The dynamics of Lumi-R might be instrumental for the further evolution of the reaction towards Meta-R by sampling multiple pathways. Such finding was only accessible by a time-resolved experiment at room temperature, because cryo-trapping procedures would freeze out specific sub-states. More generally, we note that aiding the interpretation of time-resolved infrared spectroscopy with MD simulations[61,68] may be a fruitful approach, which is not yet fully explored. The approach adds molecular detail to the interpretation of infrared spectra and can therefore be useful for the investigation of structural changes in enzymes.

Photosensory proteins are molecular machines that translate light signals into biochemical signals. Here we reveal for bacteriophytochromes, how light-induced photoisomerization of the chromophore modifies the D207:R466 salt bridge, which connects the PAS/GAF domains and the PHY tongue region, and how these changes are linked to the quaternary changes of the protein. The involved arginine and aspartate residues are strictly conserved and we therefore suggest that this mechanism may apply widely in the phytochrome superfamily. The observed structural change is a starting point for more extensive rearrangements such as tongue refolding[18,19,21] and changes in the output domains.[25] It will be interesting to see the complete molecular mechanism emerge in the future.

Materials and Methods

Details are described in SI Materials and Methods. This section includes information on expression and purification of PAS-GAF-PHY with isotopic labeling procedures, mass spectrometry, sample preparation for FTIR spectroscopy, time-resolved two-color step-scan and steady-state FTIR experiments, flash photolysis, data analysis, femtosecond pump-probe spectroscopy and MD simulations.

Supporting Information

Comparison of the hydrogen bond strength from experiments and simulations, full recovery of the Pr state, raw data from time-resolved FTIR spectroscopy, time-resolved FTIR and visible spectroscopy on dimeric *Dr*BphP$_{PSM}$, mass spectrometry data of the *Dr*BphP$_{PSM}$, difference spectra of Pfr *minus* Pr from steady-state FTIR spectroscopy, quantum chemical calculations on the downshift of the amide modes by $^{13}C^{15}N$ labeling, of the carbonyl mode of ring D by deuteration, and of the arginine and aspartate modes by $^{13}C^{15}N$ labeling, comparison between the Lumi-R spectrum in D_2O recorded by step-scan and by pump-probe infrared spectroscopy and Gaussian fit of the carbonyl region, biliverdin structure and distribution of torsion angles from the 100 ps force probe simulations, inter-atomic distances and distributions in monomer A and monomer B during four MD simulations of Lumi-R, root mean square deviation of the backbone atoms in Pr, Pfr, and Lumi-R simulations, details on the Lumi-R structure from MD simulations, movie on the dynamics of the biliverdin, R466, F469 and F198 from the B monomer of the Lumi-R phytochrome during 1000 nanoseconds of MD simulations, electric field acting on the C=O (D-ring), distributions of minimum distances from MD simulations of the Lumi-R state, FTIR signals of the backbone changes along the photocycle of *Dr*BphP$_{PSM}$, the conformational changes in the Lumi-R state, atomic charges and atom types of Pr and Pfr states of the biliverdin chromophore, atomic charges and atom types of Pr and Pfr states of the Cys24 bound to biliverdin.

Acknowledgements

Gerrit Groenhof, Heikki Takala, and Jessica Rumfeldt are acknowledged for the discussions and comments on the manuscript. Harald Förstendorf is acknowledged for providing the data of the References[30,34], and Karsten Heyne for providing us the coordinates of their

model of Lumi-R. The Computer Science Center (CSC) of Espoo, Finland, for providing computational resources for the MD simulations. The grants from Academy of Finland (296135, 266274, 304455, and 277194 for JAI, SD, VM, and HL), the Jane and Erkko foundation, and a fellowship of the Swiss National Science Foundation to B S-B (P2ZHP2_164991) are acknowledged. In particular, the Finnish Cultural Foundation is acknowledged for providing the possibility for the sabbatical leave of JAI. SW acknowledges support by the Knut and Alice Wallenberg Foundation. SW and JAI thank the Foundation of International Cooperation in Research and Higher Education. This work has been supported by a fellowship of the Studienstiftung des Deutschen Volkes to LS and a Heisenberg fellowship of the Deutsche Forschungsgemeinschaft to TK (KO3580/4-2).

References

(1) Davis, S. J.; Vener, A. V.; Vierstra, R. D. Bacteriophytochromes: Phytochrome-like Photoreceptors from Nonphotosynthetic Eubacteria. *Science* **1999**, *286* (5449), 2517–2520.

(2) Hughes, J.; Lamparter, T.; Mittmann, F.; Hartmann, E.; Gartner, W.; Wilde, A.; Borner, T. A Prokaryotic Phytochrome [6]. *Nature* **1997**, *386* (6626), 663.

(3) Yeh, K. C.; Wu, S. H.; Murphy, J. T.; Lagarias, J. C. A Cyanobacterial Phytochrome Two Component Light Regulatory Sensory System. *Science* **1997**, *277* (5331), 1505–1508.

(4) Fankhauser, C. The Phytochromes, a Family of Red/Far-Red Absorbing Photoreceptors. *J. Biol. Chem.* **2001**, *276* (15), 11453–11456.

(5) Rockwell, N. C.; Duanmu, D.; Martin, S. S.; Bachy, C.; Price, D. C.; Bhattacharya, D.; Worden, A. Z.; Lagarias, J. C. Eukaryotic Algal Phytochromes Span the Visible Spectrum. *PNAS* **2014**, *111* (10), 3871–3876.

(6) Gan, F.; Zhang, S.; Rockwell, N. C.; Martin, S. S.; Lagarias, J. C.; Bryant, D. A. Extensive Remodeling of a Cyanobacterial Photosynthetic Apparatus in Far-Red Light. *Science* **2014**, *345* (6202), 1312–1317.

(7) Legris, M.; Klose, C.; Burgie, E. S.; Rojas, C. C.; Neme, M.; Hiltbrunner, A.; Wigge, P. A.; Schäfer, E.; Vierstra, R. D.; Casal, J. J. Phytochrome B Integrates Light and Temperature Signals in Arabidopsis. *Science* **2016**, *354* (6314), 897–900.

(8) Quail, P. H. Phytochrome Photosensory Signalling Networks. *Nat. Rev. Mol. Cell Biol.* **2002**, *3* (2), 85–93.

(9) Lamparter, T.; Carrascal, M.; Michael, N.; Martinez, E.; Rottwinkel, G.; Abian, J. The Biliverdin Chromophore Binds Covalently to a Conserved Cysteine Residue in the N-Terminus of Agrobacterium Phytochrome Agp1. *Biochemistry* **2004**, *43* (12), 3659–3669.

(10) Linschitz, H.; Kasche, V. The Kinetics of Phytochrome Conversion. *J. Biol. Chem.* **1966**, *241* (14), 3395–3403.

(11) Aramendia, P. F.; Ruzsicska, B. P.; Braslavsky, S. E.; Schaffner, K. Laser Flash Photolysis of 124-Kilodalton Oat Phytochrome in H20 and D20 Solutions: Formation and Decay of the I70o Intermediates. *Biochemistry* **1987**, *26* (5), 1418–1422.

(12) Kandori, H.; Yoshihara, K.; Tokutomi, S. Primary Process of Phytochrome: Initial Step of Photomorphogenesis in Green Plants. *JACS* **1992**, *114* (27), 10958–10959.

(13) Van Thor, J. J.; Borucki, B.; Crielaard, W.; Otto, H.; Lamparter, T.; Hughes, J.; Hellingwerf, K. J.; Heyn, M. P. Light-Induced Proton Release and Proton Uptake Reactions in the Cyanobacterial Phytochrome Cph1. *Biochemistry* **2001**, *40* (38), 11460–11471.

(14) Borucki, B.; Von Stetten, D.; Seibeck, S.; Lamparter, T.; Michael, N.; Mroginski, M. A.; Otto, H.; Murgida, D. H.; Heyn, M. P.; Hildebrandt, P. Light-Induced Proton Release of Phytochrome Is Coupled to the Transient Deprotonation of the Tetrapyrrole Chromophore. *J. Biol. Chem.* **2005**, *280* (40), 34358–34364.

(15) Mathes, T.; Ravensbergen, J.; Kloz, M.; Gleichmann, T.; Gallagher, K. D.; Woitowich, N. C.; St. Peter, R.; Kovaleva, S. E.; Stojković, E. A.; Kennis, J. T. M. Femto- to Microsecond Photodynamics of an Unusual Bacteriophytochrome. *JPCL* **2015**, *6* (2), 239–243.

(16) Song, C.; Rohmer, T.; Tiersch, M.; Zaanen, J.; Hughes, J.; Matysik, J. Solid-State NMR

Spectroscopy to Probe Photoactivation in Canonical Phytochromes. *Photochem. Photobiol.* **2013**, *89* (2), 259–273.

(17) Wagner, J. R.; Brunzelle, J. S.; Forest, K. T.; Vierstra, R. D. A Light-Sensing Knot Revealed by the Structure of the Chromophore-Binding Domain of Phytochrome. *Nature* **2005**, *438* (7066), 325–331.

(18) Essen, L.-O.; Mailliet, J.; Hughes, J. The Structure of a Complete Phytochrome Sensory Module in the Pr Ground State. *PNAS* **2008**, *105* (38), 14709–14714.

(19) Yang, X.; Kuk, J.; Moffat, K. Crystal Structure of Pseudomonas Aeruginosa Bacteriophytochrome: Photoconversion and Signal Transduction. *PNAS* **2008**, *105* (38), 14715–14720.

(20) Song, C.; Psakis, G.; Lang, C.; Mailliet, J.; Gartner, W.; Hughes, J.; Matysik, J. Two Ground State Isoforms and a Chromophore D-Ring Photoflip Triggering Extensive Intramolecular Changes in a Canonical Phytochrome. *PNAS* **2011**, *108* (10), 3842–3847.

(21) Takala, H.; Björling, A.; Berntsson, O.; Lehtivuori, H.; Niebling, S.; Hoernke, M.; Kosheleva, I.; Henning, R.; Menzel, A.; Ihalainen, J. A.; Westenhoff, S. Signal Amplification and Transduction in Phytochrome Photosensors. *Nature* **2014**, *509* (7499), 245–248.

(22) Burgie, E. S.; Bussell, A. N.; Walker, J. M.; Dubiel, K.; Vierstra, R. D. Crystal Structure of the Photosensing Module from a Red/Far-Red Light-Absorbing Plant Phytochrome. *PNAS* **2014**, *111* (28), 10179–10184.

(23) Burgie, E. S.; Zhang, J.; Vierstra, R. D. Crystal Structure of Deinococcus Phytochrome in the Photoactivated State Reveals a Cascade of Structural Rearrangements during Photoconversion. *Structure* **2016**, *24* (3), 448–457.

(24) Nagano, S.; Scheerer, P.; Zubow, K.; Michael, N.; Inomata, K.; Lamparter, T.; Krauß, N. The Crystal Structures of the N-Terminal Photosensory Core Module of Agrobacterium Phytochrome Agp1 as Parallel and Anti-Parallel Dimers. *J. Biol. Chem.* **2016**, *291* (39), 20674–20691.

(25) Gourinchas, G.; Etzl, S.; Göbl, C.; Vide, U.; Madl, T.; Winkler, A. Long-Range Allosteric Signaling in Red Light–regulated Diguanylyl Cyclases. *Sci. Adv.* **2017**, *3* (3), e1602498.

(26) Yang, Y.; Linke, M.; Von Haimberger, T.; Hahn, J.; Matute, R.; González, L.; Schmieder, P.; Heyne, K. Real-Time Tracking of Phytochrome's Orientational Changes during Pr Photoisomerization. *JACS* **2012**, *134* (3), 1408–1411.

(27) Dasgupta, J.; Frontiera, R. R.; Taylor, K. C.; Lagarias, J. C.; Mathies, R. A. Ultrafast Excited-State Isomerization in Phytochrome Revealed by Femtosecond Stimulated Raman Spectroscopy. *PNAS* **2009**, *106* (6), 1784–1789.

(28) Björling, A.; Berntsson, O.; Lehtivuori, H.; Takala, H.; Hughes, A. J.; Panman, M.; Hoernke, M.; Niebling, S.; Henry, L.; Henning, R.; Kosheleva, I.; Chukharev, V.; Tkachenko, N. V.; Menzel, A.; Newby, G.; Khakhulin, D.; Wulff, M.; Ihalainen, J. A.; Westenhoff, S. Structural Photoactivation of a Full-Length Bacterial Phytochrome. *Sci. Adv.* **2016**, *2* (8), e1600920.

(29) Burgie, E. S.; Wang, T.; Bussell, A. N.; Walker, J. M.; Li, H.; Vierstra, R. D. Crystallographic and Electron Microscopic Analyses of a Bacterial Phytochrome Reveal Local and Global Rearrangements during Photoconversion. *J. Biol. Chem.* **2014**, *289* (35), 24573–24587.

(30) Foerstendorf, H.; Mummert, E.; Schäfer, E.; Scheer, H.; Siebert, F. Fourier-Transform Infrared Spectroscopy of Phytochrome: Difference Spectra of the Intermediates of the Photoreactions. *Biochemistry* **1996**, *35* (33), 10793–10799.
(31) Yang, X.; Ren, Z.; Kuk, J.; Moffat, K. Temperature-Scan Cryocrystallography Reveals Reaction Intermediates in Bacteriophytochrome. *Nature* **2011**, *479* (7373), 428–431.
(32) Rohmer, T.; Lang, C.; Bongards, C.; Gupta, K. B. S. S.; Neugebauer, J.; Hughes, J.; Gärtner, W.; Matysik, J. Phytochrome as Molecular Machine: Revealing Chromophore Action during the Pfr → Pr Photoconversion by Magic-Angle Spinning NMR Spectroscopy. *JACS* **2010**, *132* (12), 4431–4437.
(33) Eitoku, T.; Zarate, X.; Kozhukh, G. V.; Kim, J. Il; Song, P. S.; Terazima, M. Time-Resolved Detection of Conformational Changes in Oat Phytochrome A: Time-Dependent Diffusion. *Biophys. J.* **2006**, *91* (10), 3797–3804.
(34) Foerstendorf, H.; Benda, C.; Gärtner, W.; Storf, M.; Scheer, H.; Siebert, F. FTIR Studies of Phytochrome Photoreactions Reveal the C=O Bands of the Chromophore: Consequences for Its Protonation States, Conformation, and Protein Interaction. *Biochemistry* **2001**, *40* (49), 14952–14959.
(35) Schwinté, P.; Gärtner, W.; Sharda, S.; Mroginski, M. A.; Hildebrandt, P.; Siebert, F. The Photoreactions of Recombinant Phytochrome CphA from the Cyanobacterium Calothrix PCC7601: A Low-Temperature UV-Vis and FTIR Study. *Photochem. Photobiol.* **2009**, *85* (1), 239–249.
(36) Piwowarski, P.; Ritter, E.; Hofmann, K. P.; Hildebrandt, P.; von Stetten, D.; Scheerer, P.; Michael, N.; Lamparter, T.; Bartl, F. Light-Induced Activation of Bacterial Phytochrome Agp1 Monitored by Static and Time-Resolved FTIR Spectroscopy. *ChemPhysChem* **2010**, *11* (6), 1207–1214.
(37) Von Stetten, D.; Günther, M.; Scheerer, P.; Murgida, D. H.; Mroginski, M. A.; Krauß, N.; Lamparter, T.; Zhang, J.; Anstrom, D. M.; Vierstra, R. D.; Forest, K. T.; Hildebrandt, P. Chromophore Heterogeneity and Photoconversion in Phytochrome Crystals and Solution Studied by Resonance Raman Spectroscopy. *Angew. Chemie - Int. Ed.* **2008**, *47* (25), 4753–4755.
(38) Van Thor, J. J.; Ronayne, K. L.; Towrie, M. Formation of the Early Photoproduct Lumi-R of Cyanobacterial Phytochrome Cph1 Observed by Ultrafast Mid-Infrared Spectroscopy. *JACS* **2007**, *129* (1), 126–132.
(39) Uhmann, W.; Becker, A.; Taran, C.; Siebert, F. Time-Resolved FT-IR Absorption Spectroscopy Using a Step-Scan Interferometer. *Appl. Spectrosc.* **1991**, *45* (3), 390–397.
(40) Kottke, T.; Lórenz-Fonfría, V. A.; Heberle, J. The Grateful Infrared: Sequential Protein Structural Changes Resolved by Infrared Difference Spectroscopy. *J. Phys. Chem. A* **2017**, *121* (2), 335–350.
(41) Henzler-Wildman, K.; Kern, D. Dynamic Personalities of Proteins. *Nature* **2007**, *450* (7172), 964–972.
(42) Thöing, C.; Oldemeyer, S.; Kottke, T. Microsecond Deprotonation of Aspartic Acid and Response of the α/β Subdomain Precede C-Terminal Signaling in the Blue Light Sensor Plant Cryptochrome. *JACS* **2015**, *137* (18), 5990–5999.
(43) Lorenz-Fonfria, V. A.; Resler, T.; Krause, N.; Nack, M.; Gossing, M.; Fischer von Mollard, G.; Bamann, C.; Bamberg, E.; Schlesinger, R.; Heberle, J. Transient

Protonation Changes in Channelrhodopsin-2 and Their Relevance to Channel Gating. *PNAS* **2013**, *110* (14), E1273–E1281.

(44) Brudler, R.; Rammelsberg, R.; Woo, T. T.; Getzoff, E. D.; Gerwert, K. Structure of the I1 Early Intermediate of Photoactive Yellow Protein by FTIR Spectroscopy. *Nat. Struct. Biol.* **2001**, *8* (3), 265–270.

(45) Pfeifer, A.; Majerus, T.; Zikihara, K.; Matsuoka, D.; Tokutomi, S.; Heberle, J.; Kottke, T. Time-Resolved Fourier Transform Infrared Study on Photoadduct Formation and Secondary Structural Changes within the Phototropin LOV Domain. *Biophys. J.* **2009**, *96* (4), 1462–1470.

(46) Hein, M.; Wegener, A. A.; Engelhard, M.; Siebert, F. Time-Resolved FTIR Studies of Sensory Rhodopsin II (NpSRII) from Natronobacterium Pharaonis: Implications for Proton Transport and Receptor Activation. *Biophys. J.* **2003**, *84* (2 I), 1208–1217.

(47) Dioumaev, A. K.; Braiman, M. S. Nano- and Microsecond Time-Resolved FTIR Spectroscopy of the Halorhodopsin Photocycle. *Photochem. Photobiol.* **1997**, *66* (6), 755–763.

(48) Weidlich, O.; Siebert, F. Time-Resolved Step-Scan FT-IR Investigations of the Transition from KL to L in the Bacteriorhodopsin Photocycle: Identification of Chromophore Twists by Assigning Hydrogen-out-of-Plane (HOOP) Bending Vibrations. *Appl. Spectrosc.* **1993**, *47* (9), 1394–1400.

(49) Burie, J.-R.; Leibl, W.; Nabedryk, E.; Breton, J. Step-Scan FT-IR Spectroscopy of Electron Transfer in the Photosynthetic Bacterial Reaction Center. *Appl. Spectrosc.* **1993**, *47* (9), 1401–1404.

(50) Heitbrink, D.; Sigurdson, H.; Bolwien, C.; Brzezinski, P.; Heberle, J. Transient Binding of CO to CuBin Cytochrome c Oxidase Is Dynamically Linked to Structural Changes around a Carboxyl Group: A Time-Resolved Step-Scan Fourier Transform Infrared Investigation. *Biophys. J.* **2002**, *82* (1), 1–10.

(51) Björling, A.; Berntsson, O.; Takala, H.; Gallagher, K. D.; Patel, H.; Gustavsson, E.; St. Peter, R.; Duong, P.; Nugent, A.; Zhang, F.; Berntsen, P.; Appio, R.; Rajkovic, I.; Lehtivuori, H.; Panman, M. R.; Hoernke, M.; Niebling, S.; Harimoorthy, R.; Lamparter, T.; Stojkovicì, E. A.; Ihalainen, J. A.; Westenhoff, S. Ubiquitous Structural Signaling in Bacterial Phytochromes. *JPCL* **2015**, *6* (13), 3379–3383.

(52) Takala, H.; Björling, A.; Linna, M.; Westenhoff, S.; Ihalainen, J. A. Light-Induced Changes in the Dimerization Interface of Bacteriophytochromes. *J. Biol. Chem.* **2015**, *290* (26), 16383–16392.

(53) Velazquez Escobar, F.; Piwowarski, P.; Salewski, J.; Michael, N.; Fernandez Lopez, M.; Rupp, A.; Muhammad Qureshi, B.; Scheerer, P.; Bartl, F.; Frankenberg-Dinkel, N.; Siebert, F.; Andrea Mroginski, M.; Hildebrandt, P. A Protonation-Coupled Feedback Mechanism Controls the Signalling Process in Bathy Phytochromes. *Nat. Chem.* **2015**, *7* (5), 423–430.

(54) Karniol, B.; Vierstra, R. D. The Pair of Bacteriophytochromes from Agrobacterium Tumefaciens Are Histidine Kinases with Opposing Photobiological Properties. *PNAS* **2003**, *100* (5), 2807–2812.

(55) Borucki, B. Proton Transfer in the Photoreceptors Phytochrome and Photoactive Yellow Protein. *Photochem. Photobiol. Sci.* **2006**, *5* (6), 553.

(56) Braiman, M. S.; Briercheck, D. M.; Kriger, K. M. Modeling Vibrational Spectra of Amino Acid Side Chains in Proteins: Effects of Protonation State, Counterion, and

Solvent on Arginine C–N Stretch Frequencies †. *J. Phys. Chem. B* **1999**, *103* (22), 4744–4750.

(57) Barth, A.; Zscherp, C. What Vibrations Tell about Proteins. *Q. Rev. Biophys.* **2002**, *35* (4), S0033583502003815.

(58) Andresen, M.; Wahl, M. C.; Stiel, A. C.; Grater, F.; Schafer, L. V.; Trowitzsch, S.; Weber, G.; Eggeling, C.; Grubmuller, H.; Hell, S. W.; Jakobs, S. Structure and Mechanism of the Reversible Photoswitch of a Fluorescent Protein. *PNAS* **2005**, *102* (37), 13070–13074.

(59) Rockwell, N. C.; Shang, L.; Martin, S. S.; Lagarias, J. C. Distinct Classes of Red/Far-Red Photochemistry within the Phytochrome Superfamily. *PNAS* **2009**, *106* (15), 6123–6127.

(60) Lenngren, N.; Edlund, P.; Takala, H.; Stucki-Buchli, B.; Rumfeldt, J.; Peshev, I.; Häkkänen, H.; Westenhoff, S.; Ihalainen, J. A. Coordination of the Biliverdin D-Ring in Bacteriophytochromes. *Phys. Chem. Chem. Phys.* **2018**, *20* (27), 18216–18225.

(61) Fried, S. D.; Bagchi, S.; Boxer, S. G. Measuring Electrostatic Fields in Both Hydrogen-Bonding and Non-Hydrogen-Bonding Environments Using Carbonyl Vibrational Probes. *JACS* **2013**, *135* (30), 11181–11192.

(62) Goormaghtigh, E.; Ruysschaert, J. M.; Raussens, V. Evaluation of the Information Content in Infrared Spectra for Protein Secondary Structure Determination. *Biophys. J.* **2006**, *90* (8), 2946–2957.

(63) Stojković, E. A.; Toh, K. C.; Alexandre, M. T. A.; Baclayon, M.; Moffat, K.; Kennis, J. T. M. FTIR Spectroscopy Revealing Light-Dependent Refolding of the Conserved Tongue Region of Bacteriophytochrome. *JPCL* **2014**, *5* (15), 2512–2515.

(64) Takala, H.; Niebling, S.; Berntsson, O.; Björling, A.; Lehtivuori, H.; Häkkänen, H.; Panman, M.; Gustavsson, E.; Hoernke, M.; Newby, G.; Zontone, F.; Wulff, M.; Menzel, A.; Ihalainen, J. A.; Westenhoff, S. Light-Induced Structural Changes in a Monomeric Bacteriophytochrome. *Struct. Dyn.* **2016**, *3* (5), 054701.

(65) Ihalainen, J. A.; Bredenbeck, J.; Pfister, R.; Helbing, J.; Chi, L.; van Stokkum, I. H. M.; Woolley, G. A.; Hamm, P. Folding and Unfolding of a Photoswitchable Peptide from Picoseconds to Microseconds. *PNAS* **2007**, *104* (13), 5383–5388.

(66) Hauser, K.; Krejtschi, C.; Huang, R.; Wu, L.; Keiderling, T. A. Site-Specific Relaxation Kinetics of a Tryptophan Zipper Hairpin Peptide Using Temperature-Jump IR Spectroscopy and Isotopic Labeling. *JACS* **2008**, *130* (10), 2984–2992.

(67) Anders, K.; Daminelli-Widany, G.; Mroginski, M. A.; Von Stetten, D.; Essen, L. O. Structure of the Cyanobacterial Phytochrome 2 Photosensor Implies a Tryptophan Switch for Phytochrome Signaling. *J. Biol. Chem.* **2013**, *288* (50), 35714–35725.

(68) Kratochvil, H. T.; Carr, J. K.; Matulef, K.; Annen, A. W.; Li, H.; Maj, M.; Ostmeyer, J.; Serrano, A. L.; Raghuraman, H.; Moran, S. D.; Skinner, J. L.; Perozo, E.; Roux, B.; Valiyaveetil, F. I.; Zanni, M. T. Instantaneous Ion Configurations in the K+ion Channel Selectivity Filter Revealed by 2D IR Spectroscopy. *Science* **2016**, *353* (6303), 1040–1044.

Table of contents graphic